Transverse-electric Brewster effect enabled by nonmagnetic two-dimensional materials

Xiao Lin,[1,2] Yichen Shen,[2] Ido Kaminer,[2,*] Hongsheng Chen,[1,3,†] and Marin Soljačić[2]

[1]*College of Information Science and Electronic Engineering, Zhejiang University, Hangzhou 310027, China*

[2]*Department of Physics, Massachusetts Institute of Technology, Cambridge, Massachusetts 02139, USA*

[3]*The Electromagnetics Academy at Zhejiang University, State Key Laboratory of Modern Optical Instrumentation, Zhejiang University, Hangzhou 310027, China*

(Received 17 June 2016; revised manuscript received 1 August 2016; published 18 August 2016)

Discovered in the 19th century, the Brewster effect is known to occur for transverse-magnetic waves in regular optical dielectrics; however, it is believed to arise for transverse-electric (TE) waves only in systems with magnetic responses, i.e., nonunity effective relative permeability. This paper introduces a scheme to realize the TE Brewster effect in a homogeneous dielectric interface without magnetic responses, by adding ultrathin two-dimensional (2D) materials such as graphene. In particular, the effect remains even for waves approaching normal incidence, spanning from terahertz to visible frequencies. In contrast to the conventional Brewster effect, the graphene-assisted TE Brewster effect is asymmetric, and can be achieved only when the incidence is from the higher-refractive-index side. Moreover, graphene layers can tailor a total-internal-reflection dielectric interface into zero reflection, accompanied by perfect absorption. This control over TE waves enabled by ultrathin 2D materials may lead to a variety of applications, such as atomically thin absorbers, polarizers, and antireflection coating.

DOI: 10.1103/PhysRevA.94.023836

I. INTRODUCTION

Following the pioneering work of Sir David Brewster in the early 1810's [1,2], Brewster's no-reflection effect became one of the main features of the laws of reflection for electromagnetic waves. At a specific incident angle, known as the Brewster angle or polarization angle, the polarization of the reflected wave becomes independent of the incident wave [3]. When the system is slightly absorbing, a pseudo-Brewster angle can be obtained [4]. In naturally occurring dielectrics, this phenomenon exists only for transverse-magnetic (TM, or p-wave polarization) waves [3]. It is believed that the Brewster effect for transverse-electric (TE, or s-wave polarization) waves arises only for media with magnetic responses [3]; i.e., the effective relative permeability is nonunity. However, the magnetic response exhibited in natural dielectrics is typically very weak, especially for the visible frequencies. Nowadays, only the TM Brewster effect is widely used in optical devices, such as polarizers [3,5], the Brewster window in gas lasers [5], and the optical broadband angular selectivity [6–8].

Therefore, from both technological and physical points of view, it is desirable to realize the TE Brewster effect in all-dielectric systems. Recently, the advent of metamaterials [9] provides a new way to create nonunity effective relative permeability in all-dielectric systems. This led to the TE Brewster effect being experimentally reported in bulk metamaterials [10,11], and the Brewster effect being studied in magnetic [12,13], anisotropic [7,14–19], chiral [2,20], and bianisotropic [21] media. Moreover, although the Brewster effect is regarded as a phenomenon occurring at a homogeneous interface between two different bulk media, its concept has been extended to the thin metasurface through artificially tailoring the interface to be nonhomogeneous [19,22,23]. Note that in order to realize the TE Brewster effect, the unit cells in the metamaterials and metasurfaces are all designed to have strong magnetic responses [10,11,22,23]. It is still a long-standing challenge to achieve the TE Brewster effect at a homogeneous interface in all-dielectric systems without magnetic responses. In 2007, a new electromagnetic mode, known as the TE graphene plasmons [24] (different from the more famous TM graphene plasmons [25–28]), was predicted in graphene. This hints at the possibility of an alternative way of creating the TE Brewster effect that requires no magnetic responses whatsoever. Importantly, graphene, characterized by a surface conductivity σ_s [24,26–29], is just one example of many different two-dimensional (2D) materials [25,30] that can be made exceptionally thin. As we will show, a nontrivial surface conductivity is exactly what is needed for the realization of the nonmagnetic TE Brewster effect; therefore, other future 2D materials, and in particular 2D conductors, will likely further enrich the potential implementations of the TE Brewster effect.

In this paper, we introduce a scheme to obtain the TE Brewster effect spanning from THz to visible frequencies in a homogeneous interface between two different bulk dielectrics, assisted by an ultrathin 2D material (exemplified by graphene below). The underlying mechanism is that the lossy graphene, behaving as an ultrathin absorber or resistive sheet, can fully absorb the reflected TE waves. Interestingly, this can occur even for waves at zero angle of incidence, which is impossible for the conventional Brewster effect. Particularly, we show that graphene can tailor a total-internal-reflection lossless dielectric interface into a zero-reflection one, leading to the broadband high absorption of TE waves. Furthermore, due to the loss in graphene, although the system is still reciprocal, the reflection becomes asymmetric. The TE Brewster no-reflection effect thus can only be realized for incidence from the higher-refractive-index side, different from the conventional Brewster effect in lossless systems.

II. RESULTS AND DISCUSSION

In order to discuss the possible realization of the TE Brewster effect from ultrathin 2D materials, the nonmagnetic TE Brewster condition is analytically derived, which is directly

*kaminer@mit.edu

†hansomchen@zju.edu.cn

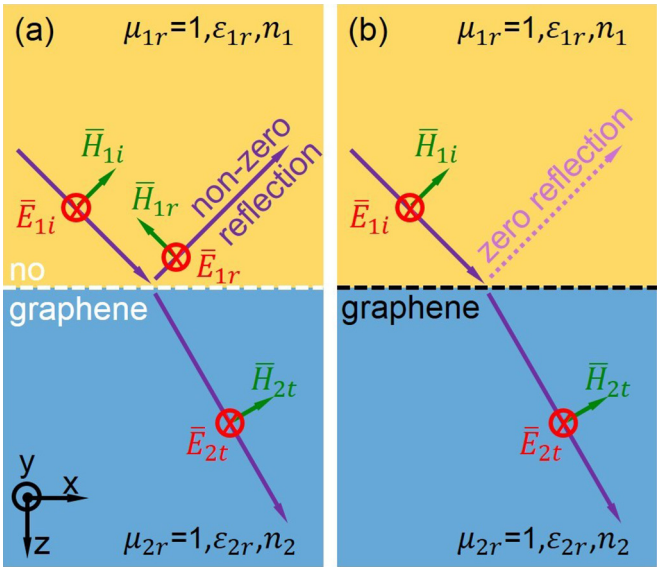

FIG. 1. Schematics of reflection and refraction of a TE wave at a homogeneous interface between two semi-infinite different dielectrics. For the TE wave, its electric field is perpendicular to the plane of incidence. (a) No graphene at the interface (white dashed line). The reflection exists. (b) With graphene at the interface (black dashed line). The reflection can disappear.

linked to the reflection coefficient. Here we assume the incidence plane to be the x-z plane and the interface between region 1 ($z < 0$) and region 2 ($z > 0$) at the plane of $z = 0$ in Fig. 1(a). For TE waves, the electric field only has the component of E_y. From the electromagnetic theory [3], one can assume the fields in each region as

$$\bar{E}_{1i} = \hat{y} e^{ik_x x} e^{+ik_{1z} z}, \tag{1a}$$

$$\bar{E}_{1r} = \hat{y} R^{\mathrm{TE}}_{1|2} e^{ik_x x} e^{-ik_{1z} z}, \tag{1b}$$

$$\bar{E}_{2t} = \hat{y} T^{\mathrm{TE}}_{1|2} e^{ik_x x} e^{+ik_{2z} z}. \tag{1c}$$

In the above, $\bar{E}_{1i}$, $\bar{E}_{1r}$, and $\bar{E}_{2t}$ are the incident, reflected, and transmitted electric fields; k_x and $k_{mz} = \sqrt{\frac{\omega^2 \varepsilon_{mr} \mu_{mr}}{c^2} - k_x^2}$ are the components of the wave vector parallel and perpendicular to the interface; $c = \frac{1}{\sqrt{\varepsilon_0 \mu_0}}$ is the speed of light; ε_{mr} and μ_{mr} are the relative permittivity and permeability; ε_0 and μ_0 are the vacuum permittivity and permeability; the region index m is equal to 1 or 2 in all the subscripts of k_{mz}, ε_{mr}, and μ_{mr}, respectively. By enforcing the boundary conditions [3], one obtains the reflection coefficient as

$$R^{\mathrm{TE}}_{1|2} = \frac{\frac{k_{1z}}{\mu_{1r}} - \sigma_s \omega \mu_0 - \frac{k_{2z}}{\mu_{2r}}}{\frac{k_{1z}}{\mu_{1r}} + \sigma_s \omega \mu_0 + \frac{k_{2z}}{\mu_{2r}}}. \tag{2}$$

Meanwhile, the transmission coefficient is $T^{\mathrm{TE}}_{1|2} = 2\frac{k_{1z}}{\mu_{1r}} / (\frac{k_{1z}}{\mu_{1r}} + \sigma_s \omega \mu_0 + \frac{k_{2z}}{\mu_{2r}})$. In the subscripts of $R^{\mathrm{TE}}_{m|j}$, we define the regions m and j as the incident and transmitted regions, respectively. Then the reflectance, transmittance, and absorbance of TE waves are defined as $r_{1|2} = |R^{\mathrm{TE}}_{1|2}|^2$, $t_{1|2} = \mathrm{Re}(\frac{k^*_{2z}/\mu^*_{2r}}{k^*_{1z}/\mu^*_{1r}} |T^{\mathrm{TE}}_{1|2}|^2)$, and $a_{1|2} = 1 - r_{1|2} - t_{1|2}$, respectively. When the TE Brewster no-reflection condition (i.e., $R^{\mathrm{TE}}_{1|2} = 0$) is fulfilled, the absorbance is $a_{1|2} = \mathrm{Re}(\frac{\sigma^*_s \omega \mu_0}{k^*_{2z}/\mu^*_{2r} + \sigma^*_s \omega \mu_0})$ and becomes significant when $|\sigma^*_s \omega \mu_0|$ is comparable to $|k^*_{2z}/\mu^*_{2r}|$. Note that due to the non-negligible absorbance, it is challenging to achieve close to unity transmittance when the nonmagnetic TE Brewster effect happens, unlike the conventional Brewster effect in lossless systems, but similar to the pseudo-Brewster effect in lossy systems [4]. According to Eq. (2), the TE Brewster no-reflection condition is derived as

$$\frac{k_{1z}}{\mu_{1r}} - \sigma_s \omega \mu_0 - \frac{k_{2z}}{\mu_{2r}} = 0. \tag{3}$$

Note that the equation that governs the dispersion of TE graphene plasmons is $\frac{k_{1z}}{\mu_{1r}} + \sigma_s \omega \mu_0 + \frac{k_{2z}}{\mu_{2r}} = 0$ [24], which is different from Eq. (3). Therefore, when the TE Brewster no-reflection condition is satisfied, the TE graphene plasmons will not be excited.

To obtain the conventional TE Brewster effect without surface conductivity, one has to have $\mu_{1r} \neq \mu_{2r}$ in order to satisfy Eq. (3). This explicitly explains the nonexistence of the TE Brewster effect in nonmagnetic systems ($\mu_{1r} = \mu_{2r} = 1$) in Fig. 1(a). However, by introducing surface conductivity, one can satisfy Eq. (3) even when $\mu_{1r} = \mu_{2r} = 1$. This way, the TE Brewster effect is enabled in a nonmagnetic system [see Fig. 1(b)]. More generally, Eq. (3) shall apply for any ultrathin material such that its electromagnetic response can be accurately described by surface conductivity. In principle, as long as the appropriate surface conductivity satisfying Eq. (3) can be found or artificially made, the nonmagnetic TE Brewster effect could be realized in the full wave spectra, ranging from microwave to even ultraviolet frequencies. Since the solution will be obtained under the condition of $k_x \ll k_F$ in Eq. (3), where $k_F = \frac{\mu_c}{\hbar v_F}$ is the Fermi wave vector, $v_F = 10^6$ m/s is the Fermi velocity, and $\hbar$ is the reduced Planck constant, respectively; the nonlocal effect in graphene is negligible [27]. It is thus reasonable to apply the local model of the Kubo formula [24,31–33] to characterize graphene's surface conductivity σ_s. We set the chemical potential as $\mu_c = 0.2$ eV, the relaxation time $\tau = 0.1$ ps, and the temperature $T = 300$ K for graphene in the following, where all these parameters are viable in realistic experiments. As can be seen from Fig. 5, while $\mathrm{Re}(\sigma_s)$ is always positive, $\mathrm{Im}(\sigma_s)$ can alternatively be positive when $\omega < 1.67\mu_c/\hbar$ or negative when $\omega > 1.67\mu_c/\hbar$ for the electron-doped graphene.

With the existence of ultrathin 2D materials, the nonmagnetic TE Brewster effect is found realizable not only under oblique incidence but also when approaching the normal incidence. When under normal incidence, since $k_{1z} = n_1 \frac{\omega}{c}$ and $k_{2z} = n_2 \frac{\omega}{c}$, Eq. (3) can be simplified to

$$\delta_n = n_1 - n_2 = \sigma_s \sqrt{\frac{\mu_0}{\varepsilon_0}}, \tag{4}$$

where $n_m = \sqrt{\varepsilon_{mr}}$ is the refractive index. Since graphene is lossy [$\mathrm{Re}(\sigma_s) > 0$], Eq. (4) requires $\mathrm{Re}(\delta_n) > 0$, indicating that the nonmagnetic TE Brewster effect under normal incidence can only be realized when incident from the higher-refractive-index side. Meanwhile, when $\mathrm{Im}(\delta_n) \geqslant 0 [\mathrm{Im}(\delta_n) < 0]$, Eq. (4) requires $\mathrm{Im}(\sigma_s) \geqslant 0 [\mathrm{Im}(\sigma_s) < 0]$, indicating that a possible solution for Eq. (4) exists in the range of $\omega \leqslant \frac{1.67\mu_c}{\hbar}$ ($\omega > \frac{1.67\mu_c}{\hbar}$). For simplicity, region 2 is set to be air with $n_2 = 1$ in the following discussion (note, however, that Fig. 4 below also demonstrates the effect for other cases).

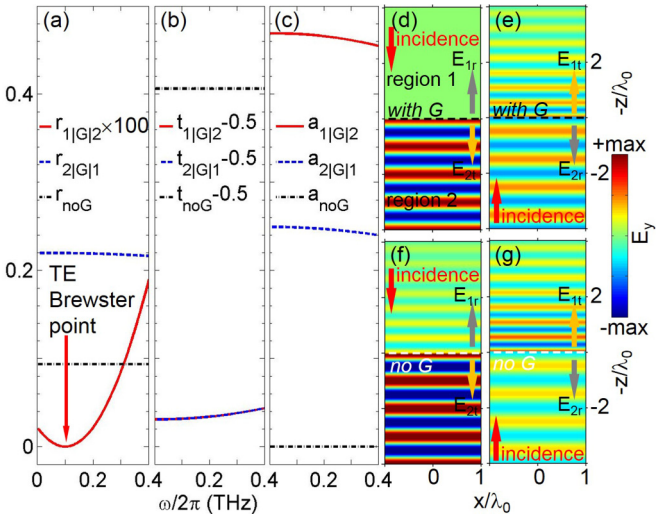

FIG. 2. THz nonmagnetic TE Brewster effect from monolayer graphene under normal incidence at 0.1 THz. The reference wavelength is $\lambda_0 = 3000\,\mu$m. The character "G" is the abbreviation for graphene. (a–c) Spectra of reflectance, transmittance, and absorbance. For the purpose of clear demonstration, the value of $r_{1|G|2}$ is multiplied by a factor of 100. (d–g) Reflected and transmitted electric fields with (d,e) and without (f,g) graphene at the dielectric interface. The incident, reflected, and transmitted directions are denoted by the red, gray, and orange arrows, respectively.

Figure 2 shows the nonmagnetic TE Brewster effect from monolayer graphene under normal incidence at 0.1 THz (i.e., the vacuum wavelength is 3000 μm). Note that under normal incidence, the TE and TM waves are degenerate. The surface conductivity of monolayer graphene at 0.1 THz is $\sigma_s = (38.5 + 2.42\mathrm{i})G_0$ (see Fig. 5), where $G_0 = \frac{e^2}{4\hbar}$ is the universal optical conductivity. One can use $n_1 = 1.88 + 0.06i$ and $n_2 = 1$ to satisfy the nonmagnetic TE Brewster condition. Figures 2(a)–2(c) show the spectra of the reflectance, transmittance, and absorbance from the interfaces with and without graphene, both when incident from region 1 and from region 2; Figs. 2(d)–2(g) show the field distributions of the reflected and transmitted electric fields at 0.1 THz. When incident from region 1, zero reflectance from the graphene-assisted interface is obtained at 0.1 THz in Figs. 2(a) and 2(d). Compared with the reflectance from the bare dielectric interface, graphene can decrease the reflectance by at least two orders of magnitude below 0.3 THz in Fig. 2(a). A negligible reflectance (<0.1%) at 0.1 THz can also be achieved in a wide range of incidence angle (<19°); see Fig. 7. This shows that graphene can potentially be used to design an atomically thin antireflection coating. Besides, the existence of graphene also degrades the transmittance in Fig. 2(b), due to its large absorbance in Fig. 2(c). This is different from the unity transmittance of the conventional Brewster effect in lossless systems. These above phenomena can be understood through the following physical process. When the TE wave is incident at the interface, it will be partly reflected. Meanwhile, it will also induce a surface current at the interface due to the existence of graphene's surface conductivity. This surface current will reemit another TE wave into region 1. Finally, the destructive interference between these two TE waves in region 1 will diminish the total reflection and also enhance the absorption at the graphene layer. We thus argue that the underlying mechanism for the graphene-assisted TE Brewster effect is that graphene can totally absorb the reflected TE wave. Interestingly, this mechanism is analogous to the impedance matching used in the design of perfect absorbers [34,35], although in our case it occurs within a single atomic layer.

Figure 2 also emphasizes the asymmetry of the system: When light is incident from region 2, the reflectance from the graphene-assisted interface becomes comparable to the one from the bare dielectric interface [see Figs. 2(e) and 2(g)], which is unlike the case when light is incident from region 1 [see Figs. 2(d) and 2(f)]. This is reasonable because while the system is still reciprocal [as can be seen from the transmittance in Fig. 2(b) which is irrelevant to the incident region, i.e., $t_{1|2} = t_{2|1}$], the lossy graphene can make the reflectance asymmetric (i.e., $r_{2|1} \neq r_{1|2}$). Note that we have $R^{\mathrm{TE}}_{2|1} = -R^{\mathrm{TE}}_{1|2}$ and $r_{2|1} = r_{1|2}$ only when graphene's surface conductivity $\sigma_s = 0$. Therefore the existence of graphene at the boundary will make the reflection asymmetric. While it was previously shown that a deeply subwavelength layer can alter the reflectance [36], in our case even a single atomic layer is sufficient for a significant change. As a conclusion from the above discussion, it follows that the graphene-assisted TE Brewster effect can be realized only when light is incident from the specific region with a larger refractive index, in contrast to the conventional Brewster effect in the lossless systems.

So far, we have presented the TE Brewster effect with the Brewster angle that is smaller than the critical angle (0° vs 32° in Fig. 7). The critical angle is the angle above which total internal reflection happens. In what comes next, we present a more intriguing case that cannot occur for the conventional Brewster angle: The TE Brewster angle can be made larger than the critical angle (see more in Figs. 8 and 11), which means that both the reflectance and transmittance can be zero. This phenomenon has only been discussed before in anisotropic left-handed metamaterials [14].

The nonmagnetic TE Brewster effect can also be implemented under oblique incidence. Under oblique incidence, Eq. (3) can be simplified to

$$\sqrt{\varepsilon_{1r} - \frac{k_x^2 c^2}{\omega^2}} - \sqrt{\varepsilon_{2r} - \frac{k_x^2 c^2}{\omega^2}} = \sigma_s \sqrt{\frac{\mu_0}{\varepsilon_0}}. \tag{5}$$

Note that in order to fulfill the nonmagnetic TE Brewster condition under normal incidence, Eq. (4) requires the materials in at least one of regions 1 and 2 to be lossy (see Fig. 2). Here, for oblique incidence, Eq. (5) allows the materials in both regions to be chosen lossless. Among various solutions of Eq. (5), here we judiciously limit ourselves to the case that the bare dielectric interface is lossless; namely, both ε_{1r} and ε_{2r} are real. This way, $\varepsilon_{1r} - \frac{k_x^2 c^2}{\omega^2}$ and $\varepsilon_{2r} - \frac{k_x^2 c^2}{\omega^2}$ in Eq. (5) are also real. Meanwhile, since the propagating plane wave is incident from region 1, one has $\varepsilon_{1r} - \frac{k_x^2 c^2}{\omega^2} \geqslant 0$ in Eq. (5). Moreover, because the passive graphene σ_s has a complex value and $\mathrm{Re}(\sigma_s) > 0$, it simultaneously requires $\varepsilon_{1r} - \frac{k_x^2 c^2}{\omega^2} > 0$ and $\varepsilon_{2r} - \frac{k_x^2 c^2}{\omega^2} \leqslant 0$ in Eq. (5), where the nonpositive real $\varepsilon_{2r} \frac{k_x^2 c^2}{\omega^2}$ in Eq. (5) will in turn demand $\mathrm{Im}(\sigma_s) \leqslant 0$. This indicates that a possible solution for the nonmagnetic TE Brewster effect under oblique incidence

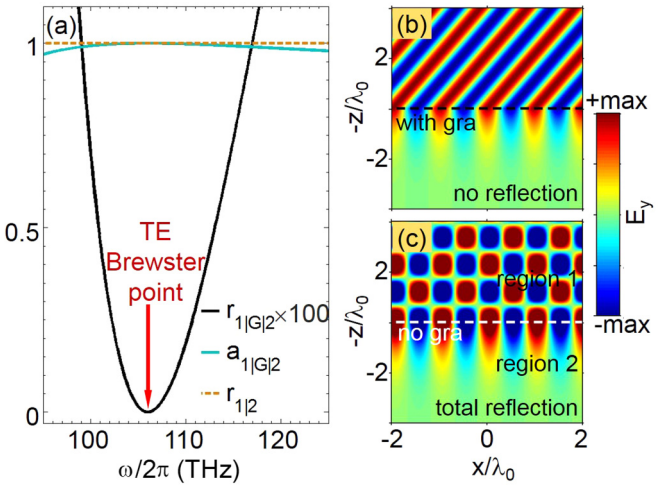

FIG. 3. Infrared nonmagnetic TE Brewster effect from multilayer graphene under oblique incidence at 106 THz. The reference wavelength is $\lambda_0 = 2.83\,\mu$m. The figure shows that graphene can tailor a total-internal-reflection lossless dielectric interface into a zero-reflection one, given the parameters are carefully tuned. (a) Spectra of reflectance and absorbance. (b,c) Total electric field in each region with (b) and without (c) graphene at the dielectric interface. The propagating TE wave is incident from region 1 with an incident angle of 65°. Here "gra" is the abbreviation for graphene.

lies within the range of $\omega \geqslant \frac{1.67\mu_c}{\hbar}$. The requirements also indicate that the total internal reflection of TE waves happens at the bare lossless dielectric interface, but the existence of graphene can tune the total internal reflection to be zero. Then Eq. (5) can be further transformed to

$$\varepsilon_{1r} - \varepsilon_{2r} = |\sigma_s|^2 \frac{\mu_0}{\varepsilon_0}. \tag{6}$$

Figure 3 shows the nonmagnetic TE Brewster effect from multilayer graphene under oblique incidence at 106 THz (i.e., the vacuum wavelength is 2.83 μm). The surface conductivity of monolayer graphene at 106 THz is $\sigma_s = (0.68 - 0.27\mathrm{i})G_0$. One should note that due to this small value of $|\sigma_s|$ of monolayer graphene in the range of $\omega > \frac{1.67\mu_c}{\hbar}$ (comparable with G_0; see Fig. 5), the value of $\varepsilon_{1r} - \varepsilon_{2r}$ satisfying Eq. (6) is very small ($\sim 5 \times 10^{-4}$). See Fig. 9 for further details. To be relevant for a larger variety of material in infrared and visible frequencies, one needs to increase the value of $\varepsilon_{1r} - \varepsilon_{2r}$. To achieve this goal, one may adopt a larger surface conductivity (e.g., Fig. 2) or use multilayer 2D materials (such as stacking 30 layers of graphene, having a thickness ~10.5 nm). It is reasonable to treat the ultrathin multilayer graphene with a layer number of N approximately as a surface conductivity of $N\sigma_s$ [37–40] (this is because for the multilayer graphene, the interlayer interaction at infrared or visible frequency is typically weak [37,38]; see Fig. 6). For example, when using 30 layers of graphene in Fig. 3, one can use $\varepsilon_{1r} = 1.25$ and $\varepsilon_{2r} = 1$ to satisfy the TE Brewster condition in Eqs. (5) and (6). Correspondingly, the TE Brewster angle is found to be larger than the critical angle (65° vs 63°; see Fig. 8), which is impossible for the conventional Brewster effect. When the dielectric interface is covered by graphene, zero reflectance and zero transmittance are obtained at 106 THz in Figs. 3(a) and 3(b), in contrast to the total internal reflection at the bare dielectric interface in Figs. 3(a) and 3(c). Moreover, the monolayer graphene can absorb over 99% of the energy of the incident TE wave over a broad frequency range from 99 to 117 THz in Fig. 3(a). This, being different from the conventional Brewster effect in lossless systems that has zero absorbance and unity transmittance, suggests a potential application of graphene as a broadband perfect absorber or an ultrathin antireflection coating, but at the same time limits the applications of such mechanism in regimes requiring unity transmission [5–8]. Note that the antireflection coating in this work is only achieved from high-index medium to low-index medium, which is less common than conventional air-to-dielectric antireflection coating. However, there are many places where eliminating reflection in the high-index-medium side is important, such as optical interconnect and fiber communication, where light is transmitted between waveguides with different refractive indexes. In addition, in contrast to the negligible reflectance of TE waves, the reflectance of TM waves over the above broad frequency range can be very high (>80%; see Fig. 12). This indicates the potential usage of our approach for optical polarizers (through the reflected wave instead of the transmitted wave).

The nonmagnetic TE Brewster effect under oblique incidence can be further extended to the visible frequency as shown in Fig. 4. This can be simply realized by using intrinsic graphene layers even without any doping (the results at this frequency range are fairly independent of the chemical potential). In order to increase the value of $\varepsilon_{1r} - \varepsilon_{2r}$, one can follow the above strategy by replacing monolayer graphene with multilayer 2D materials. We show the visible nonmagnetic TE Brewster effect under oblique incidence created by using ten layers of intrinsic graphene in Fig. 4. The surface conductivity of monolayer graphene without electron doping is $\sigma_s = (1.42 - 0.78i)G_0$ at 603 THz (i.e., the photon energy is 2.5 eV or the vacuum wavelength is 497 nm); see Fig. 6. The setup of $\varepsilon_{1r} = 2.14$ and $\varepsilon_{2r} = 2$ would satisfy the TE Brewster

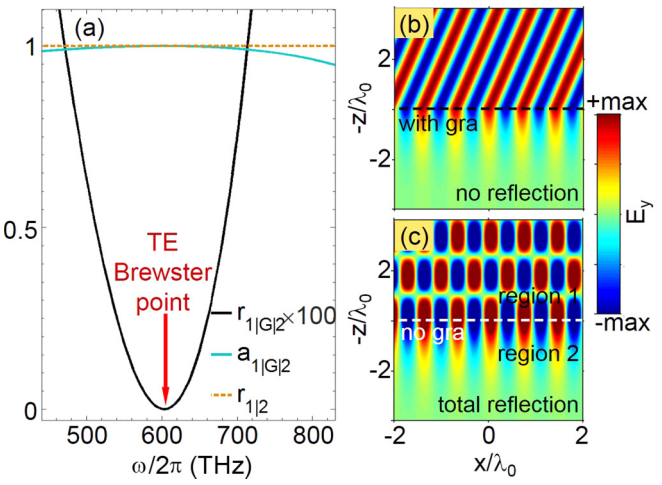

FIG. 4. Visible nonmagnetic TE Brewster effect created by using multilayer graphene without electron doping under oblique incidence at 603 THz. The reference wavelength is $\lambda_0 = 497$ nm. (a) Spectra of reflectance and absorbance. (b,c) Total electric field in each region with (b) and without (c) graphene at the dielectric interface. The propagating TE wave is incident from region 1 with an incident angle of 77°.

condition of Eqs. (5) and (6). The resultant Brewster angle is found to be larger than the critical angle (77° vs 75°; see more in Fig. 11). For a vivid understanding, we schematically demonstrate the visible nonmagnetic TE Brewster effect from ten layers of intrinsic graphene at 603 THz in Fig. 4(b). All these results in Fig. 4 reveal the possible design of visible optical devices (such as polarizers) from 2D materials, where the use of intrinsic graphene layers shall provide more feasibility in practical experiments.

As shown above, a nontrivial surface conductivity is the key requirement for the realization of the nonmagnetic TE Brewster effect. Therefore, in addition to graphene, other 2D materials or ultrathin conductors [25,30] (which can be accurately modeled by a surface conductivity) can also be applied to enrich the implementations of the nonmagnetic TE Brewster effect. However, we argue that graphene is especially suitable for this purpose because of the technological advances in the fabrication of large-area and high-quality samples, in the precise control of the atomic-layer number, and in the flexible adjustment of the chemical potential.

III. CONCLUSION

We propose an approach for realizing the nonmagnetic TE Brewster effect under both normal and oblique incidences in a 2D-material-assisted dielectric interface spanning terahertz, infrared, and visible frequencies. The 2D-material-assisted TE Brewster effect is asymmetric, achieving zero reflection only for incidence from the higher-refractive-index side. Unlike the conventional Brewster angle that always appears below the critical angle of the total internal reflection, we reveal that the 2D-material-assisted TE Brewster angle can appear above the critical angle, exhibiting total absorption. Due to the abundance of 2D materials, our proof-of-concept results show that the 2D-material-assisted nonmagnetic TE Brewster effect can be of significance to the development of unique THz-to-visible optical devices with miniaturized size and improved functionality, such as atomically thin antireflection coatings, tunable optical polarizers, and broadband perfect absorbers.

ACKNOWLEDGMENTS

This work was sponsored by the National Natural Science Foundation of China under Grants No. 61322501, No. 61574127, and No. 61275183, the Top-Notch Young Talents Program of China, the Program for New Century Excellent Talents (Program No. NCET-12-0489) in University, the Fundamental Research Funds for the Central Universities, the Innovation Joint Research Center for Cyber-Physical-Society System, and the US Army Research Laboratory and the US Army Research Office through the Institute for Soldier Nanotechnologies (Contract No. W911NF-13-D-0001). M.S. was supported in part (reading and analysis of the manuscript) by the MIT S3TEC Energy Research Frontier Center of the Department of Energy under Grant No. DESC0001299. X.L. was supported by the Chinese Scholarship Council (CSC No. 201506320075). I.K. was partially supported by the Seventh Framework Programme of the European Research Council (FP7-Marie Curie IOF) under Grant No. 328853-MC-BSiCS.

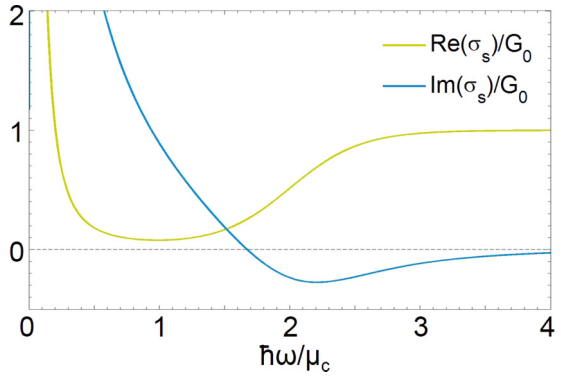

FIG. 5. Surface conductivity of monolayer graphene calculated by the Kubo formula [24,31,32,35], i.e., $\sigma_s(\omega,\mu_c,\tau,T) = \frac{-ie^2(\omega+i/\tau)}{\pi\hbar^2}\{\frac{1}{(\omega+i/\tau)^2}\int_0^{+\infty} x_E[\frac{\partial f_d(x_E)}{\partial x_E} - \frac{\partial f_d(-x_E)}{\partial x_E}]dx_E - \int_0^{+\infty}\frac{f_d(-x_E)-f_d(x_E)}{(\omega+i/\tau)^2-4(x_E/\hbar)^2}dx_E\}$ where e is the elementary charge, $f_d(E) = (e^{\frac{E-\mu_c}{k_BT}}+1)^{-1}$ is the Fermi-Dirac distribution, and k_B is Boltzmann's constant. Here we set the temperature $T = 300\,\mathrm{K}$, the relaxation time $\tau = 0.1\,\mathrm{ps}$, and the chemical potential in graphene $\mu_c = 0.2\,\mathrm{eV}$. While the real part of graphene's surface conductivity $\mathrm{Re}(\sigma_s)$ is positive, its imaginary part $\mathrm{Im}(\sigma_s)$ changes from positive to negative at $\omega = 1.67\mu_c/\hbar$.

APPENDIX A: DERIVATION OF REFLECTION FOR TE WAVES

The detailed derivation of the reflection coefficient of TE waves in Eq. (2) is given in this Appendix. Once the electric

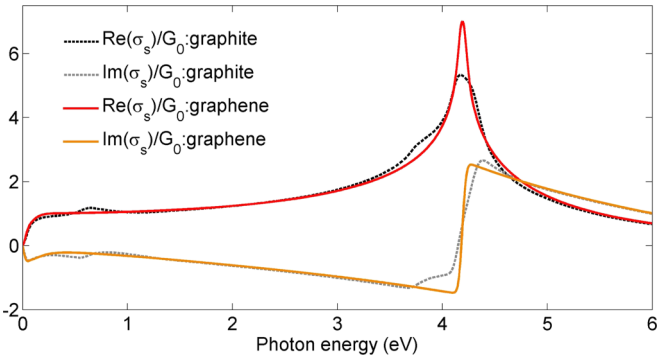

FIG. 6. Surface conductivity of intrinsic monolayer graphene and each graphene layer in the bulk graphite, calculated from the density functional theory (DFT) by using the commercial SIESTA software [37,41]. We assume there is no electron doping in both monolayer graphene and the bulk graphite. The photon energy of 1 eV corresponds to the photon frequency of 241 THz. The surface conductivities in the monolayer graphene and each graphene layer in the bulk graphite have negligible differences within the photon energy range of 1–3.2 eV, and have relatively slight differences below 1.0 eV due to the interlayer interaction. As a demonstration of concept, we neglect the difference between graphene's surface conductivity and the averaged surface conductivity of each layer in the multilayer graphene (such as 30 layers of graphene) at 106 THz (i.e., the photon energy is 0.44 eV) (see Fig. 3 in the main text). From Fig. 6, we can safely argue that the surface conductivity of multilayer graphene with a layer number of N is N times the surface conductivity of monolayer graphene in the visible frequency range (400–720 THz; i.e., the corresponding range of photon energy is 1.66–2.98 eV) (see Fig. 4 in the main text).

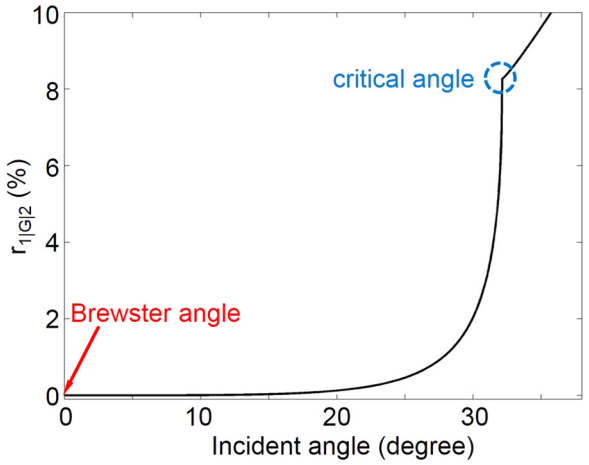

FIG. 7. TE wave reflectance from monolayer graphene as a function of the incident angle at 0.1 THz. Graphene is assumed to be located at the dielectric interface between regions 1 and 2. The TE wave is incident from region 1. The refractive indexes of regions 1 and 2 are $n_1 = 1.88 + 0.06i$ and $n_2 = 1$, respectively. We set the chemical potential $\mu_c = 0.2$ eV, the temperature $T = 300$ K, and the relaxation time $\tau = 0.1$ ps in graphene. The character "G" is the abbreviation for graphene. When the incident angle is approaching the Brewster angle (denoted by the red arrow), the reflectance goes to zero. When the incident angle is approaching the critical angle (denoted by the dashed circle), above which the total internal reflection happens at the bare interface, a kink in the reflectance curve shows up. The Brewster angle is smaller than the critical angle (0° vs 32°).

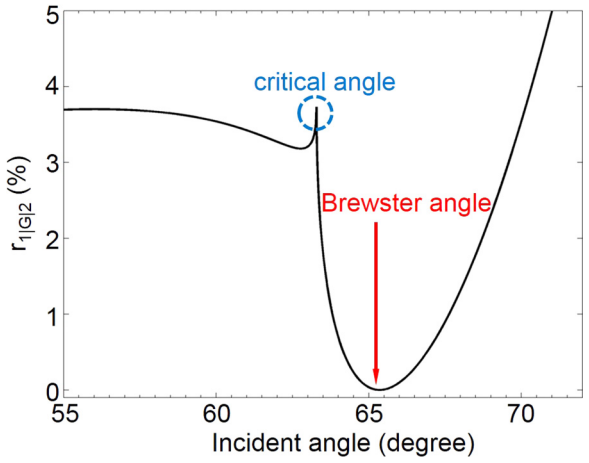

FIG. 8. TE waves reflectance from 30-layer graphene, as a function of the incident angle at 106 THz. The TE wave is incident from region 1. Graphene is assumed to be located at the dielectric interface between regions 1 and 2. The TE wave is incident from region 1. The relative permittivities in regions 1 and 2 are $\varepsilon_{1r} = 1.25$ and $\varepsilon_{2r} = 1$, respectively. We set the chemical potential $\mu_c = 0.2$ eV, the temperature $T = 300$ K, and the relaxation time $\tau = 0.1$ ps in graphene. When the incident angle is approaching the Brewster angle, the reflectance goes to zero. When the incident angle is approaching the critical angle, a peak of the reflectance shows up. Note that here the Brewster angle is larger than the critical angle (65° vs 63°), different from the case studied in Fig. 7 and from the conventional Brewster effects.

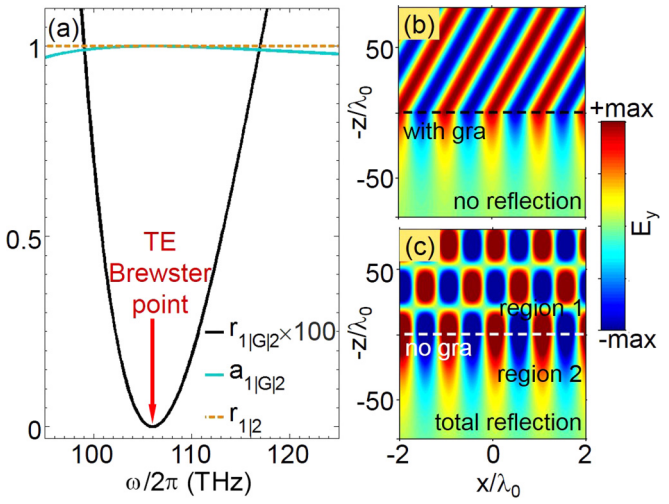

FIG. 9. Infrared nonmagnetic TE Brewster effect created by using monolayer of graphene under oblique incidence at 106 THz. The reference wavelength is $\lambda_0 = 2.83\,\mu$m. The relative permittivities in nonmagnetic regions 1 and 2 are $\varepsilon_{1r} = 1.000\,28$ and $\varepsilon_{2r} = 1$, respectively. We set the chemical potential $\mu_c = 0.2$ eV, the temperature $T = 300$ K, and the relaxation time $\tau = 0.1$ ps in graphene. (a) Spectra of reflectance and absorbance. The value of $r_{1|G|2}$ is multiplied by a factor of 100. (b–c) Total electric field in each region with (b) and without (c) graphene at the dielectric interface. The propagating TE wave is incident from region 1 with an incident angle of 89.1°. For a clear demonstration, the scale on the y axis is compressed in (b,c), compared with that of the x axis. Note that the curves in Fig. 9(a) are the same as the curves in Fig. 3(a). This is because when satisfying the nonmagnetic TE Brewster conditions of Eqs. (5) and (6) in the main text, the reflection coefficient of TE waves in Eq. (2) in the main text is only a function of the surface conductivity of monolayer graphene, independent of the graphene's layer number.

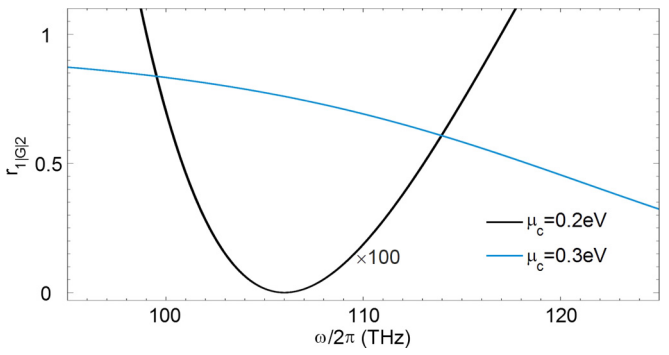

FIG. 10. Tunable TE wave reflectance from monolayer graphene through varying the chemical potential. The propagating TE wave is incident from region 1 with an incident angle of 89.1°. The other parameters are the same as those in Fig. 9. For the purpose of clear demonstration, the black line is multiplied by a factor of 100. Since the chemical potential in graphene can be flexibly tunable through the electrostatic gating, it is advantageous to use graphene to design tunable optical devices. The negligible reflectance ({<}1%) over the broad frequency range (99–117 THz) would become significant (>50%) when tuning the chemical potential of graphene from 0.2 to 0.3 eV. This suggests that graphene might be used as a real-time tunable ultrathin antireflection coating.

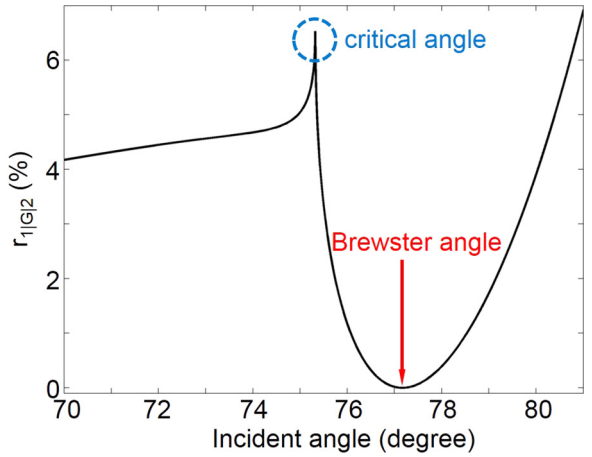

FIG. 11. TE wave reflectance from ten layers of graphene without electron doping as a function of the incident angle at 603 THz. Graphene is located at the dielectric interface between regions 1 and 2. The TE wave is incident from region 1. The relative permittivities in regions 1 and 2 are $\varepsilon_{1r} = 2.14$ and $\varepsilon_{2r} = 2$, respectively. When the incident angle is approaching the Brewster angle the reflectance goes to zero. When the incident angle is approaching the critical angle a peak of the reflectance shows up. Note that the Brewster angle is larger than the critical angle (77° vs 75°), similar to the case studied in Fig. 8.

field in each region is known, the magnetic fields can be calculated by using $\nabla \times \bar{H} = \frac{\partial(\varepsilon \bar{E})}{\partial t}$ [3]. From Eq. (1), we can write the incident magnetic field as $\bar{H}_{1i} = \frac{1}{\omega\mu_0\mu_{1r}}(\hat{z}k_x - \hat{x}k_{1z})e^{ik_x x}e^{+ik_{1z}z}$, the reflected magnetic field as $\bar{H}_{1r} = \frac{1}{\omega\mu_0\mu_{1r}}(\hat{z}k_x + \hat{x}k_{1z})R^{\rm TE}_{1|2}e^{ik_x x}e^{-ik_{1z}z}$, and the transmitted magnetic field as $\bar{H}_{2t} = \frac{1}{\omega\mu_0\mu_{2r}}(\hat{z}k_x - \hat{x}k_{2z})T^{\rm TE}_{1|2}e^{ik_x x}e^{+ik_{2z}z}$. At the boundary of $z = 0$, the boundary conditions require that $\hat{n} \times (\bar{H}_{1i} + \bar{H}_{1r} - \bar{H}_{2t}) = \bar{J}_s$ and $\hat{n} \times (\bar{E}_{1i} + \bar{E}_{1r} - \bar{E}_{2t}) = 0$ [3], where $\hat{n} = -\hat{z}$ and the surface current density $\bar{J}_s = \sigma_s \bar{E}_2|_{z=0}$. By enforcing the boundary conditions, we

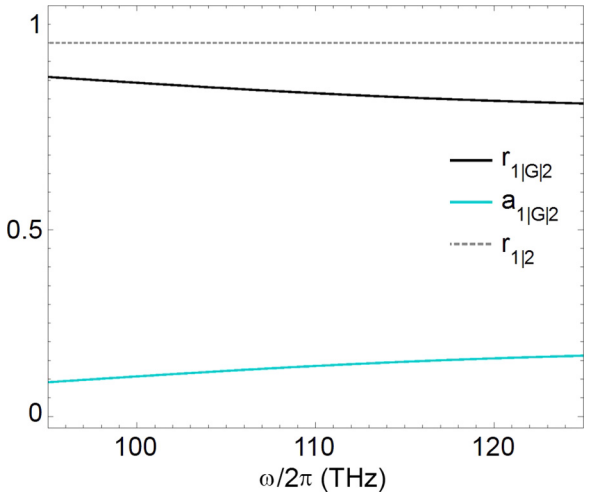

FIG. 12. Infrared TM waves reflectance and absorbance from 30-layer graphene. The parameters and setup are the same as those in Fig. 8.

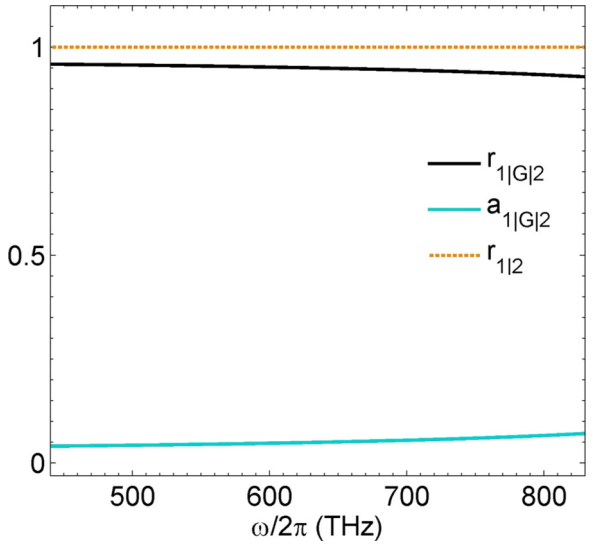

FIG. 13. Visible TM wave reflectance and absorbance from ten layers of graphene without electron doping. Graphene is located at the dielectric interface between regions 1 and 2. The propagating TM wave is incident from region 1 with an incident angle of 77°. The other parameters are the same as those in Fig. 11.

have $1 + R^{\rm TE}_{1|2} = T^{\rm TE}_{1|2}$ and $\frac{k_{1z}}{\omega\mu_0\mu_{1r}}(1 - R^{\rm TE}_{1|2}) - \frac{k_{2z}}{\omega\mu_0\mu_{2r}}T^{\rm TE}_{1|2} = \sigma_s T^{\rm TE}_{1|2}$. By solving these two equations, we obtain $R^{\rm TE}_{1|2} = (\frac{k_{1z}}{\mu_{1r}} - \sigma_s\omega\mu_0 - \frac{k_{2z}}{\mu_{2r}})/(\frac{k_{1z}}{\mu_{1r}} + \sigma_s\omega\mu_0 + \frac{k_{2z}}{\mu_{2r}})$ and $T^{\rm TE}_{1|2} = 2\frac{k_{1z}}{\mu_{1r}}/(\frac{k_{1z}}{\mu_{1r}} + \sigma_s\omega\mu_0 + \frac{k_{2z}}{\mu_{2r}})$. The time-averaged Poynting vectors for the power of the incident, reflected, and transmitted waves in the z direction at $z = 0$ are calculated to be $\langle S_{iz}\rangle = \frac{1}{2}{\rm Re}\{\frac{k^*_{1z}}{\omega\mu_0\mu^*_{1r}}\}$, $\langle S_{rz}\rangle = \frac{1}{2}{\rm Re}\{\frac{k^*_{1z}}{\omega\mu_0\mu^*_{1r}}|R^{\rm TE}_{1|2}|^2\}$, and $\langle S_{tz}\rangle = \frac{1}{2}{\rm Re}\{\frac{k^*_{2z}}{\omega\mu_0\mu^*_{2r}}|T^{\rm TE}_{1|2}|^2\}$ [3], respectively. Then the reflectance, transmittance, and absorbance of TE waves are defined as $r_{1|2} = \frac{\langle S_{rz}\rangle}{\langle S_{iz}\rangle} = |R^{\rm TE}_{1|2}|^2$, $t_{1|2} = \frac{\langle S_{tz}\rangle}{\langle S_{iz}\rangle} = {\rm Re}(\frac{k^*_{2z}/\mu^*_{2r}}{k^*_{1z}/\mu^*_{1r}}|T^{\rm TE}_{1|2}|^2)$, and $a_{1|2} = 1 - r_{1|2} - t_{1|2}$, respectively.

By following the above procedure, when the TE wave is incident from region 2, we can also obtain $R^{\rm TE}_{2|1} = (\frac{k_{2z}}{\mu_{1r}} - \sigma_s\omega\mu_0 - \frac{k_{1z}}{\mu_{1r}})/(\frac{k_{1z}}{\mu_{1r}} + \sigma_s\omega\mu_0 + \frac{k_{2z}}{\mu_{2r}})$ and $T^{\rm TE}_{2|1} = 2\frac{k_{2z}}{\mu_{2r}}/(\frac{k_{1z}}{\mu_{1r}} + \sigma_s\omega\mu_0 + \frac{k_{2z}}{\mu_{2r}})$; $r_{2|1} = |R^{\rm TE}_{2|1}|^2$, $t_{2|1} = {\rm Re}(\frac{k^*_{1z}/\mu^*_{1r}}{k^*_{2z}/\mu^*_{2r}}|T^{\rm TE}_{2|1}|^2)$, and $a_{2|1} = 1 - r_{2|1} - t_{2|1}$.

APPENDIX B: SURFACE CONDUCTIVITY OF GRAPHENE

In this appendix, we show the surface conductivity calculated by using local Kubo formula in Fig. 5 and simulated by using the commercial software SIESTA in Fig. 6.

APPENDIX C: GRAPHENE-BASED TE BREWSTER EFFECT

In this appendix, we show more information on the graphene-based TE Brewster effect, including the reflectance for TE waves in Figs. 7, 8 and 9–11 and the reflectance for TM waves in Figs. 12 and 13.

[1] D. Brewster, Philos. Trans. R. Soc. London **105**, 125 (1815).
[2] A. Lakhtakia, Opt. News **15**, 14 (1989).
[3] J. A. Kong, *Electromagnetic Wave Theory* (EMW Publishing, Cambridge, MA, 2008).
[4] S. Y. Kim and K. Vedam, J. Opt. Soc. Am. A **3**, 1772 (1986).
[5] E. Hecht, *Optics* (Addison Wesley, Reading, MA, 2002).
[6] Y. Shen, D. Ye, I. Celanovic, S. G. Johnson, J. D. Joannopoulos, and M. Soljačić, Science **343**, 1499 (2014).
[7] Y. Shen, D. Ye, L. Wang, I. Celanovic, L. Ran, J. D. Joannopoulos, and M. M. Soljacic, Phys. Rev. B **90**, 125422 (2014).
[8] Y. Shen, C. Hsu, Y. Yeng, J. D. Joannopoulos, and M. Soljačić, Appl. Phys. Rev. **3**, 011103 (2016).
[9] D. R. Smith, J. B. Pendry, and M. C. K. Wiltshire, Science **305**, 788 (2004).
[10] Y. Tamayama, T. Nakanishi, K. Sugiyama, and M. Kitano, Phys. Rev. B **73**, 193104 (2006).
[11] R. Watanabe, M. Iwanaga, and T. Ishihara, Phys. Status Solidi **245**, 2696 (2008).
[12] W. T. Doyle, Am. J. Phys. **48**, 643 (1980).
[13] J. Futterman, Am. J. Phys. **63**, 471 (1995).
[14] T. M. Grzegorczyk, Z. M. Thomas, and J. A. Kong, Appl. Phys. Lett. **86**, 251909 (2005).
[15] T. Tanaka, A. Ishikawa, and S. Kawata, Phys. Rev. B **73**, 125423 (2006).
[16] A. Alu, G. D'Aguanno, N. Mattiucci, and M. J. Bloemer, Phys. Rev. Lett. **106**, 123902 (2011).
[17] C. Argyropoulos, G. D'Aguanno, N. Mattiucci, N. Akoztek, M. J. Bloemer, and A. Alu, Phys. Rev. B **85**, 024304 (2012).
[18] K. Q. Le, C. Argyropoulos, N. Mattiucci, G. D'Aguanno, M. J. Bloemer, and A. Alu, J. Appl. Phys. **112**, 094317 (2012).
[19] C. Argyropoulos, K. Q. Le, N. Mattiucci, G. D'Aguanno, and A. Alu, Phys. Rev. B **87**, 205112 (2013).
[20] S. Bassiri, C. H. Papas, and N. Engheta, J. Opt. Soc. Am. A **5**, 1450 (1988).
[21] A. Lakhtakia, Optik **90**, 184 (1992).
[22] Y. Tamayama, Opt. Lett. **40**, 1382 (2015).
[23] R. P. Dominguez, Y. F. Yu, A. E. Miroschnichenko, L. A. Krivitsky, Y. H. Fu, V. Valuckas, L. Gonzaga, Y. T. Toh, A. Y. S. Kay, B. Lukyanchuk, and A. I. Kuznetsov, Nat. Commun. **7**, 10362 (2016).
[24] S. A. Mikhailov and K. Ziegler, Phys. Rev. Lett. **99**, 016803 (2007).
[25] F. Xia, H. Wang, D. Xiao, M. Dubey, and A. Ramasubramaniam, Nat. Photon. **8**, 899 (2014).
[26] A. N. Grigorenko, M. Polini, and K. S. Novoselov, Nat. Photon. **6**, 749 (2012).
[27] M. Jablan, H. Buljan, and M. Soljacic, Phys. Rev. B **80**, 245435 (2009).
[28] F. H. L. Koppens, D. E. Chang, and F. J. García de Abajo, Nano Lett. **11**, 3370 (2011).
[29] A. Vakil and N. Engheta, Science **332**, 1291 (2011).
[30] M. Xu, T. Liang, M. Shi, and H. Chen, Chem. Rev. **113**, 3766 (2013).
[31] V. P. Gusynin, S. G. Sharapov, and J. P. Carbotte, Phys. Rev. Lett. **96**, 256802 (2006).
[32] L. A. Falkovsky and A. A. Varlamov, Eur. Phys. J. B **56**, 281 (2007).
[33] C. A. Valagiannopoulos, A. Tukiainen, T. Aho, T. Niemi, M. Guina, S. A. Tretyakov, and C. R. Simovski, Phys. Rev. B **91**, 115305 (2015).
[34] Y. Ra'di, C. R. Simovski, and S. A. Tretyakov, Phys. Rev. Appl. **3**, 037001 (2015).
[35] G. W. Hanson, J. Appl. Phys. **103**, 064302 (2008).
[36] H. Herzig Sheinfux, I. Kaminer, Y. Plotnik, G. Bartal, and M. Segev, Phys. Rev. Lett. **113**, 243901 (2014).
[37] X. Lin, Y. Xu, A. A. Hakro, T. Hasan, R. Hao, B. Zhang, and H. Chen, J. Mater. Chem. C **1**, 1618 (2013).
[38] D. A. Smirnova1, I. V. Shadrivov, A. I. Smirnov, and Y. S. Kivshar, Laser Photon. Rev. **8**, 291 (2014).
[39] C. Casiraghi, A. Hartschuh, E. Lidorikis, H. Qian, H. Harutyunyan, T. Gokus, K. S. Novoselov, and A. C. Ferrari, Nano Lett. **7**, 2711 (2007).
[40] H. Yan, X. Li, B. Chandra, G. Tulevski, Y. Wu, M. Freitag, W. Zhu, P. Avouris, and F. Xia, Nat. Nanotechnol. **7**, 330 (2012).
[41] X. Lin, S. Lin, Y. Xu, A. A. Hakro, T. Hasan, B. Zhang, B. Yu, J. Luo, E. Li, and H. Chen, J. Mater. Chem. C **1**, 2131 (2013).